

# Effective Potentials for Liquid Water Using Polarizable and Nonpolarizable Models

A. Wallqvist and B. J. Berne\*

Department of Chemistry and Center for Biomolecular Simulation, Columbia University,  
New York, New York 10027

Received: July 30, 1993\*

Two three-site potentials for use in liquid water simulations are constructed using effective interactions. The rigid molecule has interaction centers located at atomic sites coinciding with the gas-phase monomer geometry. One potential uses solely pairwise additive potential functions whereas the other includes polarization contributions. These functions and parameters are adjusted to give simulated liquid properties at room temperature that resemble the experimental values for structure, energy, and pressure. The models presented correspond to a reduced effective representation of liquid water interactions and are labeled RER(pair) and RER(pol). Thus, the local structure of the liquid is reproduced based on the pair correlation functions for atom pairs. Analysis of dynamical properties gives a diffusion coefficient of  $2.4 \times 10^{-5}$  and  $2.8 \times 10^{-5}$  cm<sup>2</sup>/s for the nonpolarizable and polarizable model, respectively, results which can be compared with an experimental value of  $2.4 \times 10^{-5}$  cm<sup>2</sup>/s determined by Krynicki et al. [*Discuss. Faraday Soc.* 1978, 66]. Reorientational relaxation times are also in general agreement with the available experimental data, with the polarizable model exhibiting somewhat faster overall dynamics than the nonpolarizable potential. The temperature dependence of the models was also investigated in the liquid state between 250 and 350 K. The proposed models are computationally efficient and represent a viable alternative to other simple pairwise and polarizable three-center liquid water potentials.

## 1. Introduction

The study of liquid water systems using computer simulations and molecular models of water continues to be of great interest due to the ubiquitous nature of water.<sup>1–3</sup> Even with more than 20 years of experience with liquid water models, a single model that satisfactorily captures all of the essential experimental features of water has yet to be found.<sup>4–8</sup> Finding such a potential function for water may in practice not be possible due to the varied set of density, temperature, and pressure conditions that are experimentally interesting.

What makes water such an interesting and still hard-to-model fluid is a combination of strong directional polar interactions and a network of specifically arranged hydrogen bonds.<sup>9</sup> The water monomer has a permanent dipole moment of 1.85 D and a polarizability of  $1.44 \text{ \AA}^3$ . Thus, a large part of the attractive electrostatic interactions arises from polarization of molecules in the liquid. Induction effects cannot be decomposed into pairwise additive contributions as the induced moment on any one water molecule depends on all other surrounding water molecules. The liquid phase of water differs from simple fluids in that there is a large qualitative remnant of the ice structure, not in the form of local frozen patches but as tetrahedral ordering of next-nearest neighbors of water. From an enthalpic point of view, an optimum water configuration is one in which each water molecule is surrounded by four nearest neighbors forming the corners of a tetrahedron.<sup>1</sup> In the liquid phase, entropy destabilizes these conformations and the four nearest neighbors are not locked in the tetrahedral arrangement. Instead, they fluctuate around this geometry allowing molecules to penetrate and diffuse away, but the underlying tetrahedral network of hydrogen bonds does not disappear.<sup>10</sup> This network is present in water solutions even up to extreme conditions where the pressure exceeds 10 kbar.<sup>11–13</sup>

Given the extensive experimental knowledge of liquid water and the continuing interest in aqueous systems, analyzing and improving effective potential models remains important. In this work we have two aims: first, to find as simple a representation as possible for water interactions that is compatible with an all-atom model, and second, to explore polarization effects by

developing potentials that give the correct liquid-state energies, pressure, and structure using either a pair potential or a many-body representation of induction effects. In our reduced representation of liquid water, we were forced to give up the simple Bernal–Fowler type of potential.<sup>9</sup> In order to satisfactorily reproduce liquid water properties, we have introduced potential functions related to the central force models of Lemberg, Stillinger, and Rahman.<sup>14–16</sup>

A further motivation for this study was to develop a simple and malleable potential function representation of the nonelectrostatic part of water interactions for use in atom-based flexible charge models.<sup>17</sup> The available parameters and functional expressions for simple models of water are not satisfactory in this respect.<sup>18</sup>

## 2. Potential Model Development

Given the multitude of different water potentials, it is obvious that the potential parameter space is broad and that several choices of coefficients and intramolecular geometry do reproduce the tetrahedral structure of liquid water. Attractive and repulsive forces must be carefully balanced for each model in order to give a final set of parameters. These parameters are not transferable between different models but represent the set of approximations made in the construction of the potential. In this section we review the simplifications and justifications used in developing our liquid water potentials.

In the framework of classical mechanics it is possible to allow for intramolecular vibrations. Changes in the intramolecular geometry of water molecules in the liquid due to flexibility can always be modeled by an average rigid geometry.<sup>19</sup> Thus, flexibility *per se* does not introduce any new insight into liquid water, though of course a changed average geometry does.<sup>20,21</sup> Most investigations of flexibility also lack a correct description of the dependence of the polarizability and multipole moments<sup>22–26</sup> as well as dispersion and exchange parameters<sup>27</sup> on vibrational displacements. Consequently, we will consider only rigid water models.

Also implicit in the classical approach is that electronic degrees of freedom have already been averaged over, which may at best be an approximation for hydrogen atoms. Part of this approx-

\* Abstract published in *Advance ACS Abstracts*, December 1, 1993.

imation can be put back in water simulations<sup>28,29</sup> using path integral techniques, although this is not done here.

**2.1. Effective Pair Potentials.** For an assembly of  $N$  molecules it is always possible to divide the total energy into contributions arising from pairs, triplets, etc., of molecules:

$$U(\mathbf{R}_{1\dots N}) = \sum_{ij}^N V_2(\{\mathbf{R}_i\}, \{\mathbf{R}_j\}) + \sum_{ijk}^N V_3(\{\mathbf{R}_i\}, \{\mathbf{R}_j\}, \{\mathbf{R}_k\}) + \dots \quad (1)$$

In this notation,  $\mathbf{R}_{1\dots N}$  corresponds to all molecular coordinates and  $\{\mathbf{R}_i\}$  denotes the individual coordinates of the  $i$ th rigid molecule.  $V_2, V_3, \dots$  respectively denote the two-body, three-body, ... potential. A truncation of the energy expansion at the pair term is usually not feasible for water systems because of the presence of important many-body contributions. Assigning an explicit form to the  $V_3$  term and subsequent parametrization have been attempted for water from *ab initio* quantum chemistry calculations,<sup>30–34</sup> but such terms have not been generally adopted.

The nature of the true pair potential,  $V_2$ , can be examined through a perturbation expansion,<sup>35–37</sup> into electrostatic, exchange repulsion, induction, and dispersion force components. The complexity of this surface grows rapidly with the demand of accurately reproducing the total potential surface. The strict division of these energies is usually not possible, and at short distances the energy contributions become mixed. In an effective potential they are always mixed, because attractive and repulsive forces are being balanced to reproduce experimentally determined properties of the system. In this approach, at most two initial nonvanishing moments of the charge distribution are reproduced. Whether or not this is adequate cannot solely be determined from liquid simulations, because changes in the charge distribution—depending on the environment—cannot be accounted for. The dispersion interactions cannot be described only by a  $r^{-6}$  power law as this is only the leading asymptotic term in a more complex expansion of the dispersion interactions. Both short- and long-range corrections are commonly left out of the treatment. Three-body correction terms, Axilrod–Teller terms,<sup>38</sup> which are crucial for reproducing rare-gas properties, have never been implemented in water simulations. The magnitude of these correction terms can be evaluated only from accurate potentials derived through perturbation techniques. Highly accurate *ab initio* potentials give little insight into these problems, and the conversion of these data points to a simplified potential surface often overlooks these problems. In essence, such potential constructions tend to take into account environment-dependent factors by using a specific set of potential functions. The technique of parametrizing analytical potential functions from *ab initio* derived data is the major obstacle in the successful, routine implementation of these types of potentials.

Due to the highly polar nature of water it was recognized early on that adopting an effective pair potential, which incorporates many-body effects, in an average way might be more expeditious than explicitly including  $V_3$  and higher-order terms in the potential expansion. An effective potential assumes an implicit density dependence of the interaction model, because the potential incorporates the averaged influence of its immediate surroundings. In essence, a “mean field” approximation is implicitly used but never formally constructed. Thus, the total energy is approximated as

$$U(\mathbf{R}_{1\dots N}) \approx \sum_{ij}^N V_{\text{eff}}(\{\mathbf{R}_i\}, \{\mathbf{R}_j\}) \quad (2)$$

Due to the computational advantages of using a pairwise additive potential, the earliest water models uniformly included polarization induction through an effective potential.<sup>39,40</sup> Thus, such a set of pair interactions does not correspond to the true dimer potential  $V_2$ . This approach has worked surprisingly well for liquid water properties as well as for mixtures including nonpolar and polar solutes. It is actually hard to pinpoint any

specific, calculated property of liquid water at NTP that can be shown to be explicitly wrong due to the omission of nonadditive polarization terms. It is only for the dimer that a comparison between the measured values of the dimer energies clearly shows the discrepancy between the true pair potential and an effective pair potential.<sup>41</sup> An effective pair potential always overestimates the attractive energies and tends to predict the formation of dimers that are too closely bound compared to the experimental values. The oxygen–oxygen distance in the dimer energy minimum of the effective potential incorrectly corresponds to typical water pair distance found in the liquid, though the orientations are quite different between the two phases.

Many-body polarization effects can be included directly in the evaluation of the potential energy by assigning a polarizability to the water molecule. The electrical fields from the partial charges combined with the fields arising from the induced moment are then allowed to polarize a water molecule self-consistently. Thus, the total energy is written as

$$U(\mathbf{R}_{1\dots N}) \approx \sum_{ij}^N V'_{\text{eff}}(\{\mathbf{R}_i\}, \{\mathbf{R}_j\}) + V_{\text{pol}}(\mathbf{R}_{1\dots N}) \quad (3)$$

This approach picks up all three- and higher-body corrections arising from dipole polarization. Higher-order corrections in other moments or other types of interactions are not included; e.g. the changes in the electron distribution upon polarization are not trivial.<sup>42</sup> A number of polarizable water potentials have been developed and investigated using molecular dynamics or Monte Carlo simulations.<sup>43–55</sup>

**2.2. Position of Interaction Sites.** The number and location of interaction sites used to represent a water molecule vary significantly among the available water potentials. All models assign a site for an isotropic dispersion interaction to the oxygen atom. Usually this site is also a center for an exchange repulsion term. Given the high density of electrons at the oxygen atom, this site representation is a reasonable first approximation. In order to improve the representation of these forces, it is possible either to go to more refined potential function expressions<sup>4</sup> or to use a multicenter expansion<sup>56</sup> with additional sites.

A multicenter expression where point charges represent the charge distribution of the molecules is computationally efficient and circumvents the problem of using high-order and ill-determined multiple moments. The representation of the charge density is crucial for liquid water. First of all, the effective dipole moment has to be assigned. For a polarizable model choosing the gas-phase moment is convenient but neglects nuclear polarization effects in the liquid. For a nonpolarizable model, induction effects must be included in the charges assigned to the sites. The sites of these charges need not coincide with the atomic nuclei; indeed, most models either have off-atomic site charges or use a combination of more than three sites. Of course, only two charges are needed to set the dipole moment, but given the symmetry of the water molecule, three is the smallest number of charges ever employed. Three charge site models with off-atomic locations are among the most popular and widespread potential models, e.g., RWK,<sup>4,57,58</sup> MCY,<sup>59</sup> TIP4P,<sup>60</sup> and WK,<sup>61</sup> which all have a negative charge that does not coincide with the position of the oxygen atom. The SPC model<sup>62,63</sup> assigns charges to atomic sites but uses an unrealistic water monomer structure. We use the equilibrium gas-phase geometry for the water monomer in this work. Displacement of the charge distribution from the atom locations allows for a better modeling of the quadrupole moment. It has been argued,<sup>51,61</sup> that an accurate modeling of the quadrupole moment is necessary to reproduce the tetrahedral structure of liquid water. For an effective pair potential this may be sufficient, but is certainly not necessary, as it is the combination of all energy terms that determines the liquid structure. For a true pair potential, as calculated from *ab initio* quantum chemistry calculations or perturbation theory, modeling of the electrostatic energy necessitates a good description of the charge distribution

up to the quadrupole level.<sup>64</sup> Using even higher-order moments might be necessary for certain configurations,<sup>65</sup> radically increasing the number of partial charge sites needed to describe these moments.<sup>66</sup>

In recognition of the difficulty of adequately representing the true charge distribution at all distances, we choose to base our potential functions on three centers located at the atomic positions in the monomer conformation, i.e., with a bond length of 0.96 Å and a bond angle of 104.52°. Most force fields used in biomolecular simulations are also based on atom-centered potentials, giving the possibility of including our new potentials in such calculations. Another compelling reason to use as few interaction centers as possible is to reduce the computational cost. If potential functions are evaluated using a look-up procedure,<sup>67</sup> all three-site models require the same time penalty in evaluating energies and forces from a given configuration.

**2.3. Assigned Dipole Moments,  $\mu_{\text{eff}}$ .** The values of assigned dipole moments for effective water potentials range from gas-phase values of 1.85 to 2.6 D. The spread in moments reflects two things: first, there is a variation in nonelectrostatic parameters depending on the location of interaction sites as well as on the choice of experimental properties used in the fit; second, it has only lately been recognized that there is a missing component in all effective pair potentials that corresponds to the energy cost of charging the gas-phase dipole moment to its full effective value in the liquid.<sup>68</sup> The charging energy creates a large imbalance in the energy scale of polar-polar interactions when one uses these potential models directly in biomolecular force fields. Total energies must contain this energetic correction term if non-gas-phase charges are used. Thus, the SPC/E<sup>68</sup> and WK<sup>61</sup> potentials are parametrized with relatively larger effective dipole moments than are commonly used, in order to reproduce the liquid-state energies. Thus, in recognition of the good dielectric properties given by the WK model,<sup>61</sup> the early results of the polarizable electrodipole model,<sup>44</sup> the value of the molecular dipole moment of ice,<sup>69</sup> and the recent results using polarizable models, which all seem to indicate a total molecular dipole moment around 2.5–2.9 D, we assign a dipole moment of 2.6 D. Thus, for the nonpolarizable model a negative charge of  $-0.92e$  was located at the oxygen site and two charges of  $+0.46e$  at each of the hydrogen sites. The charges for the polarizable model were chosen so that the gas-phase dipole moment is 1.85 D.<sup>70</sup> The position of the atomic charges were kept fixed, even though they may change in the liquid due to nuclear polarization.

The quadrupole moment, in units of  $\text{esu cm}^2$ , for the nonpolarizable potential is  $Q_{xx} = 1.95$ ,  $Q_{yy} = -1.87$ , and  $Q_{zz} = -0.08$ , whereas for the polarizable model  $Q_{xx} = 1.39$ ,  $Q_{yy} = -1.33$ , and  $Q_{zz} = -0.06$ , compared with the experimental values<sup>71</sup>  $Q_{xx} = 2.63$ ,  $Q_{yy} = -2.50$ , and  $Q_{zz} = -0.13$ . The resultant monomer quadrupole moments are 25% and 50% lower for the RER(pair) and RER(pol) models, respectively, than the experimentally determined gas-phase values.

**2.4. Potential Energy of Nonpolarizable Models.** For an assembly of molecules with effective dipole moments different from the gas-phase values, it is necessary to include in the total electrostatic interaction energy the energy required to charge the dipole moments.<sup>72–74,61,68</sup> On the other hand, when using a polarizable model, we automatically take into account this self-energy.<sup>47,75</sup> The energy needed to create one induced dipole moment,  $\vec{\mu}$ , in a field,  $\vec{E}$ , is given by

$$V_{\text{self}} = \int_0^{\vec{\mu}} \vec{E} \cdot d\vec{\mu} = \int_0^{\vec{\mu}} \frac{\vec{\mu}}{\alpha} \cdot d\vec{\mu} = \mu^2/2\alpha \quad (4)$$

where  $\alpha$  is the molecular polarizability. For a pairwise additive potential description with an assigned dipole moment of  $\mu_{\text{eff}}$  and an associated gas-phase dipole-moment of  $\mu_{\text{gas}}$ , the correction energy can easily be calculated from the above equation by setting

the induced moment equal to

$$\mu = \mu_{\text{eff}} - \mu_{\text{gas}} \quad (5)$$

A further correction for the fluctuations of the dipole moment was introduced by Watanabe and Klein<sup>61</sup> and approximated as

$$V_{\text{flu}} = \frac{3kT}{2} \left( \frac{\mu_{\text{eff}}}{\mu_{\text{gas}}} - 1 \right) \quad (6)$$

The self-energy correction in nonpolarizable liquid water is not difficult to implement as it is just an added constant in the total energy expression. For the case of  $\mu_{\text{eff}} = 2.6$  D at 300 K,  $V_{\text{self}} = 11.7$  kJ/mol and  $V_{\text{flu}} = 1.5$  kJ/mol. If one is to use an effective water potential together with other polar molecules, also derived as effective potentials, it will be crucial to correct for the self-energy term of all molecules in order to get the relative energy scale correct. For polar molecules undergoing dihedral motion and changing their effective dipole moments, it is not clear how best to include this correction.

**2.5. Potential Energy of Polarizable Models.** The explicit inclusion of electrical polarization requires the evaluation of the induced dipole moments, which for a point polarizable molecule is given by the *total* electrical field dotted into the polarizability tensor. Because anisotropy of the polarizability tensor is 8% in water,<sup>76</sup> the approximation of using a spherical tensor is not expected to introduce any qualitative difference for the liquid state. The density dependence of the polarizability<sup>77</sup> will also be ignored. The induced dipole moment of the *i*th water is then given by

$$\vec{\mu}_i = \alpha \vec{E}_i = \alpha \{ \vec{E}_i^0 + \sum_{j \neq i}^N \vec{T}_{ij} \cdot \vec{\mu}_j \} \quad (7)$$

where the Coloumb field generated by the fixed partial charges is given by

$$\vec{E}_i^0 = \sum_{j \neq i}^N q_j \vec{r}_{ij} / 4\pi\epsilon_0 r_{ij}^3 \quad (8)$$

and the dipole tensor is defined as

$$\vec{T}_{ij} = (3\vec{r}_i \vec{r}_j - \delta_{ij} r_{ij}^2) / 4\pi\epsilon_0 r_{ij}^5 \quad (9)$$

The total energy associated with the induced dipole moments of *N* rigid water molecules, including the cost of creating them in the given external field, is simply given by

$$V_{\text{pol}}(\mathbf{R}_{1\dots N}) = -1/2 \sum_i^N \vec{E}_i^0 \cdot \vec{\mu}_i \quad (10)$$

Two main methods have been developed for the solution of these equations: iterative methods in which eq 7 is successively solved until the induced moments have converted to a self-consistent values, and a Lagrangian formulation in which the induced moment is introduced as an additive variable or coordinate.<sup>46,78</sup> We have used an iterative/predictor method developed earlier,<sup>47</sup> resulting in a time penalty for the current polarizable potential of roughly twice that of the pairwise additive potential. An alternate way of including self-consistent polarization effects in molecular modeling is to use a flexible charge model.<sup>17,18</sup>

**2.6. Choice of  $V_{\text{eff}}$  and  $V_{\text{eff}}$ .** Introduction of complexities in a potential function is warranted only if there are physically compelling reasons for it; otherwise simplicity is preferred. For effective potentials, the interpretation of the potential function itself may not be meaningful as it is only the observable, or phase space averages, that have physical meaning. Thus, the choice itself of the potential functions becomes arbitrary, and we are free to choose the number of interaction sites as well as the functional representation for all interactions. This free choice of different functional forms has been exploited by many authors.

When using an atom-based three-center model combined with a Lennard-Jones expression for the nonelectrostatic interactions,

TABLE I: Potential Parameters<sup>a</sup>

potential	$q_O, e$	$q_H, e$	$\alpha, \text{\AA}^3$	$C_{12}, \text{kJ}/(\text{mol } \text{\AA}^{12})$	$C_6, \text{kJ}/(\text{mol } \text{\AA}^6)$	$C_4, \text{kJ}/(\text{mol } \text{\AA}^4)$	$C_1, \text{kJ}/\text{mol}$	$w_1, \text{\AA}^{-2}$	$r_1, \text{\AA}$
RER(pair)	-0.920	0.460	0.00	3 500 000	-3100	15.0	-1.000	1.5	4.5
RER(pol)	-0.654	0.327	1.44	3 500 000	-3100	82.5	-2.375	1.5	4.5

<sup>a</sup> The monomer geometry for both potentials is given by a bond length  $r_0 = 0.96 \text{\AA}$  and a bond angle  $\theta_0 = 104.52^\circ$ . In order to recover the potential energy in kJ/mol when using eq 11,  $1/4\pi\epsilon_0$  should be set to 1389.0.

the  $\epsilon$ - $\sigma$  parameter space of the Lennard-Jones potential that gives tetrahedral structure invariably shifts the first peak of the oxygen-oxygen pair distribution function  $0.1 \text{\AA}$  inward, from the experimental position. In order to avoid this, we decided to add two terms to the usual water interaction representation which uses a Lennard-Jones plus partial charge terms as suggested by Bernal and Fowler.<sup>9</sup> The two new terms are a  $r^{-4}$  and a Gaussian term, which are designed to give us additional flexibility in the fitting procedure by simultaneously allowing us to control structural, energetic, and pressures of the model system. The addition of the Gaussian was inspired by the central force potentials introduced by Lemberg, Stillinger, and Rahman.<sup>14-16</sup> Thus, the functional choice of the effective pair potential is given as

$$V_{\text{eff}}(\{\mathbf{R}_i\}, \{\mathbf{R}_j\}) = \frac{C_{12}}{r_{OO}^{12}} + \frac{C_6}{r_{OO}^6} + \frac{C_4}{r_{OO}^4} + C_1 e^{-w_1(r_{OO}-r_1)^2} + \sum_{\alpha \in i, \beta \in j} \frac{q_\alpha q_\beta}{4\pi\epsilon_0 r_{\alpha\beta}} \quad (11)$$

In order to simplify the construction of the polarizable model, the same functional form was retained for the effective potential  $V_{\text{eff}}$ . The choice of the functional form of  $V_{\text{eff}}$  and  $V'_{\text{eff}}$  is not unique.

**2.7. Parametrization of Potentials.** One must parametrize the potential to capture the essential features of liquid water at room temperature. Given that there is always some uncertainty associated with experimental quantities, aiming for an exact reproduction of any one set of data is neither desirable nor warranted.

For the nonpolarizable potential, we proceeded from the given effective charge distribution to initially search the  $C_{12}$  and  $C_6$  space for parameters that give the correct size of the model molecule. This was done with a set of short simulations of 5 ps in duration to give the rough structural properties of the model liquid. If one is to improve on the location of the first oxygen-oxygen peak in the radial distribution function, it is necessary to move out of the region in the  $C_{12}$  and  $C_6$  parameter space that gives strong tetrahedral coordination. Tetrahedrality is manifested by the appearance of a second peak in the oxygen-oxygen radial distribution function. Optimally this peak should be located at  $1.6\sigma'$ , where  $\sigma'$  is the position of the first peak. The heightened tetrahedral coordination was reintroduced with the Gaussian term fitted with the  $C_1$ ,  $w_1$ , and  $r_1$  parameters in eq 11. Finally, the energy and pressure were fitted by adjusting the  $C_4$  parameter. The resulting values are given in Table I. In the case of the polarizable model, the *a priori* assumption is that the monomer dipole moment is 1.85 D and that the induction is described by an isotropic point polarizability of  $1.44 \text{\AA}^3$  located at the oxygen nucleus. Since we want the molecular dimensions to remain similar to the nonpolarizable case, the  $C_{12}$  and  $C_6$  parameters were left as they were. In order to bring the potential model in agreement with the nonpolarizable model, the  $C_4$  and  $C_1$  parameters were again refitted from a set of short simulations. The final values are given in Table I where we have labeled the nonpolarizable model potential RER(pair) and the polarizable model potential RER(pol). These labels are acronyms for reduced effective representation (RER) potentials and indicate how the induction energy is calculated: through an enhanced effective dipole moment using pairwise additive potential functions (pair) or using a self-consistent dipole polarization scheme (pol).

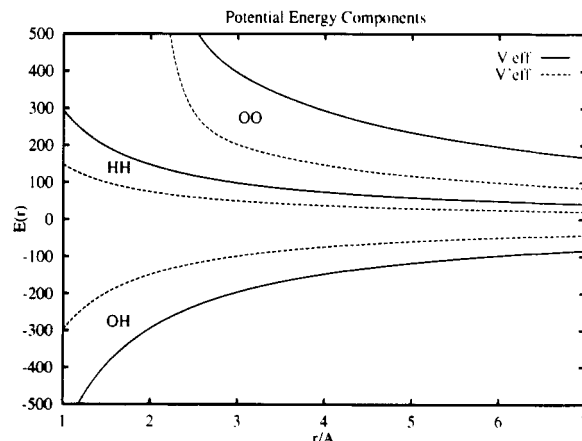
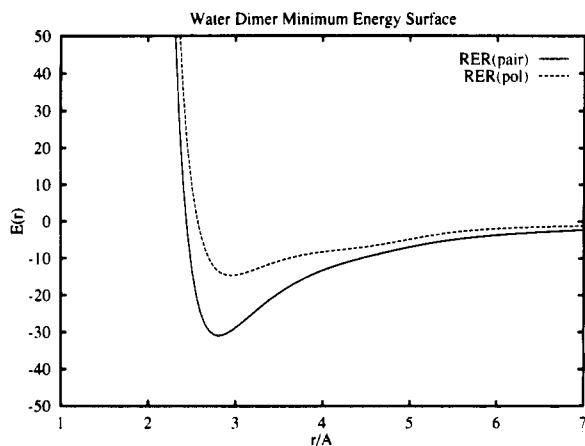


Figure 1. Atom-atom components of the effective pair potential,  $V_{\text{eff}}$  and  $V'_{\text{eff}}$  in units of kJ/mol. The two top curves refer to the pairwise oxygen-oxygen interaction, the two middle curves to the hydrogen-hydrogen interaction, and the two bottom curves to the attractive oxygen-hydrogen interaction.

The  $C_4$  and  $C_1$ ,  $w_1$ ,  $r_1$  parameters are in essence the density-dependent variables that we have utilized in fine tuning the potential for the liquid state. It is doubtful that these parameters have any physical meaning individually, although the  $C_4$  term could nominally correspond to isotropic corrections of the charge-octopole and dipole-quadrupole interaction. The  $C_1$  term serves to sharpen the tetrahedral hydrogen-bonding pattern of liquid water. Even though the model is hydrogen-bonded in a tetrahedral arrangement without the Gaussian term, the clear division into a well-separated second maximum in the oxygen-oxygen pair distribution function requires the addition of the Gaussian term.

The atomic site decomposition of the effective pair potential in terms of oxygen-oxygen, oxygen-hydrogen, and hydrogen-hydrogen interactions are drawn in Figure 1 for both models. The dominating potential term in both potentials are the electrostatic contributions. The reduction of the partial charges in the polarizable potential reflects the induction energy that has to be recouped by the many-body polarization calculation using eqs 7 and 10. As can be seen from Figure 1, this is a substantial amount, on the order of  $10^2$  kJ/mol, for each component.

**2.8. Characterization of the Dimer.** A more convenient way to categorize these different effective potentials is by their dimer minimum-energy surfaces. These surfaces are defined as those proton donor and acceptor angles that minimize the potential energy of the water dimer for a given oxygen-oxygen, or center of mass, distance. For pairwise additive potentials this surface almost invariably gives a direct mapping to liquid-state properties such as the total energy and the relative distance between nearest-neighboring water molecules. The minimum-energy surface is given in Figure 2 for both potentials. The induction energy is included in the polarizable potential, whereas the correction terms  $V_{\text{self}}$  and  $V_{\text{flu}}$  are left out of the nonpolarizable potential in Figure 2. Thus, there are the actual surfaces that are employed in the calculation of forces used in the molecular dynamics simulations. The deviations at long range reflect the different dipole moments assigned to the nonpolarizable and polarizable monomer. At shorter range the potentials are quite different, owing to the way in which the effective interactions have been taken into account. If one were to include the liquid-state correction factors of  $V_{\text{self}}$  and  $V_{\text{flu}}$  in the RER(pair) curve, this would uniformly shift the values but not bring the two curves in Figure 2 into agreement.



**Figure 2.** Dimer minimum-energy surface for the RER(pair) and RER(pol) models in units of kJ/mol. At each oxygen–oxygen distance the acceptor and donor angles have been optimized with respect to the potential energy.

**TABLE II: Dimer Structure**

potential	$r_{\min}$ , Å	$\beta_d$ , deg	$\beta_a$ , deg
RER(pair) <sup>a</sup>	2.80	48	21
RER(pol) <sup>a</sup>	2.95	47	19
SPC/E <sup>b</sup>	2.75	52	22
PSPC <sup>c</sup>	2.78	52	17
NEMO <sup>d</sup>	2.85	59	73
ASP <sup>e</sup>	2.98	52	63
experiment <sup>f</sup>	2.98	51 ± 10	57 ± 10

<sup>a</sup> This work. <sup>b</sup> Berendsen, H. J. C.; Grigera, J. R.; Straatsma, T. P. *J. Phys. Chem.* **1987**, *91*, 6296. <sup>c</sup> Ahlstrom, P.; Wallqvist, A.; Engstrom, S.; Jonsson, B. *Mol. Phys.* **1989**, *68*, 563. <sup>d</sup> Wallqvist, A.; Karlstrom, G. *Chem. Scr.* **1989**, *29A*, 131. <sup>e</sup> Millot, C.; Stone, A. J. *Mol. Phys.* **1992**, *77*, 439. <sup>f</sup> Odutola, J. A.; Dyke, T. R. *J. Chem. Phys.* **1980**, *72*, 5062.

The structure<sup>79</sup> and energetics<sup>80</sup> of the dimer have been characterized experimentally. Extensive quantum chemical calculations have also been performed on various dimer configurations.<sup>81,82</sup> Although the potentials developed here are primarily designed for condensed phases, it is still interesting to compare dimer properties. In Table II, structural data for the energy-optimized dimer configuration are gathered for some water potentials. In general, the nonpolarizable models tend to predict a too-contracted dimer. Polarizable models, can on the other hand, allow for an extended gas-phase dimer separation while induction effects will increase the dimer interaction in the liquid. The orientation of the dimer is similar for both our models and the SPC-derived potentials. It is only when a more accurate description of the charge distribution is made, as in the NEMO<sup>51</sup> and ASP<sup>65</sup> potential, that the acceptor angle takes on the experimental values.

The global minimum dimer energies found in Figure 2 is  $-30.9$  and  $-14.7$  kJ/mol for the RER(pair) and the RER(pol) models, respectively. The minimum energy for the RER(pair) potential is similar to that of the SPC/E model, which has a value of  $-29.1$  kJ/mol. Quantum chemical many-body perturbation results<sup>81</sup> indicate a value of  $-19.7 \pm 1.5$  kJ/mol for the geometry-optimized dimer. The experimental results from thermal conductivity measurements<sup>80</sup> are derived from the measured enthalpy at 373 K of  $-15.1 \pm 2.1$  kJ/mol and corrected for the differences in vibrational, rotational, and translation energy as well as a PV term to yield a dimer energy of  $-22.8 \pm 2.9$  kJ/mol. Since the nonpolarizable potentials have little meaning outside the liquid state, it is not surprising that their dimer energies show a large artificial enhancement of the binding energy. Correcting the nonpolarizable values for the  $V_{\text{self}}$  term brings the SPC/E values closer to the experimental values due to the fact that the assigned dipole moment of SPC/E,  $\mu_{\text{eff}} = 2.35$  D, is closer to the actual dipole moment in the dimer<sup>70</sup> than the RER(pair) model presented here, which has  $\mu_{\text{eff}} = 2.6$  D. Nominally, the polarizable potential should give a better description of low-density systems. The dimer

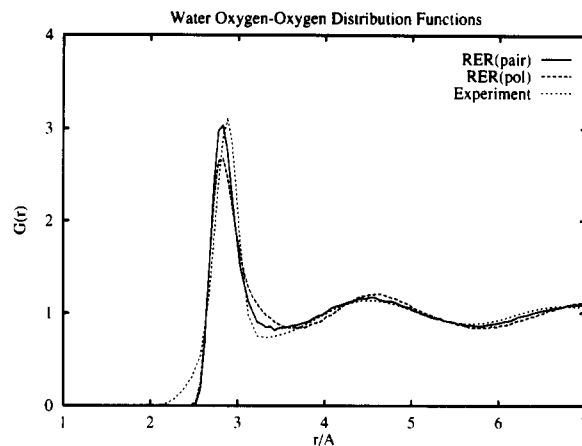


**Figure 3.** Oxygen–oxygen radial distribution function of liquid water using the developed potentials compared to an experimental data set.<sup>95</sup>

energy is too low compared with the *ab initio* results and with the measured values; even if we remove the  $C_4$  and the much smaller  $C_i$  correction terms, we only get a fair estimate of the binding energy as  $-15.9$  kJ/mol. Charge-transfer terms and quadrupolar and higher polarizabilities as well as intramolecular distortions may also contribute to the dimer minimum energy.

### 3. Liquid Water Simulations

In the simulation of liquid water systems we have used 216 water molecules enclosed in a periodically replicated cubic box. The length of the box was set to 18.6 Å, resulting in a density of 1.0 g/cm<sup>3</sup>. The equations of motions were integrated using the Rattle version<sup>83</sup> of the velocity Verlet algorithm<sup>84</sup> in order to maintain the internal bond lengths and bond angle constraints of the rigid molecule. The time step was conservatively set to 1.0 fs. Typically, the simulations covered a 25-ps equilibration period followed by a 50-ps sampling period during which averages were accumulated. Temperatures were maintained at room temperature values by periodically rescaling the velocities. Both the translational and rotational temperatures were monitored so as to avoid a temperature imbalance between these degrees of freedom. All interactions were spherically truncated at half the box length, which has been shown to be adequate in order to account for the long-range interactions.<sup>85</sup>

**3.1. Structural Properties.** Liquid water structure,<sup>86</sup> determined by X-ray<sup>87–89</sup> and neutron<sup>90–95</sup> diffraction experiments, constitutes one of the most important comparisons between simulated and real water systems. The local ordering present in liquid water does resemble an ice structure, but without the long-range ordering present in the ice crystal. The coordination number in the liquid phase is also higher than for the ice phase. Thus, it is essential for water models that the local ordering be present in the liquid phase. In Figure 3 we compare the oxygen–oxygen radial distribution function for our potentials with the data set of Soper and Phillips.<sup>95</sup> Overall, we can see that the agreement is good; the simulated liquid captures both the size of a molecule and the local tetrahedral ordering of water molecules. The height of the first oxygen–oxygen peak varies somewhat between different experimental data sets, but lies in the vicinity of 2.6–3.0. We note that the polarizable potential has incorporated the density change by shifting the peak position inward compared with the preferred dimer distances given in Table II. No such shift is observable for the nonpolarizable model. The initial slow rise of the experimental oxygen–oxygen pair distribution function has no classical analog, as *ab initio* pair energies calculated for dimer complexes,<sup>64,96</sup> at these distances would predict a very low probability of finding such complexes in the liquid. The shape of this peak is sensitive to the data transformation of X-ray data; it is also influenced by the truncation scheme in  $k$  space.<sup>97</sup>

The number of nearest water neighbors within 3.3 Å, i.e., the minimum in the experimental distribution function, is 4.5 for

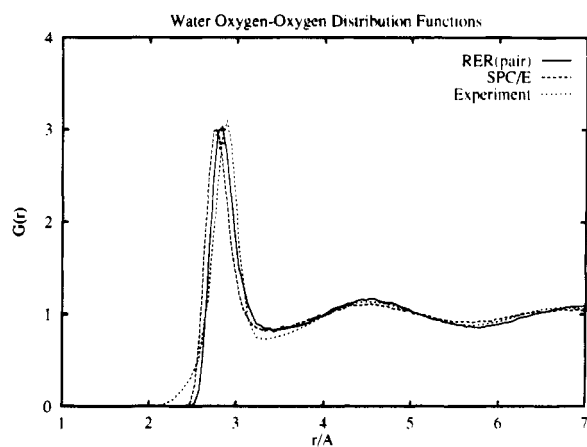


**Figure 4.** Oxygen–oxygen radial distribution function of liquid water for the RER(pair) and SPC/E<sup>68</sup> models compared to an experimental data set.<sup>95</sup>

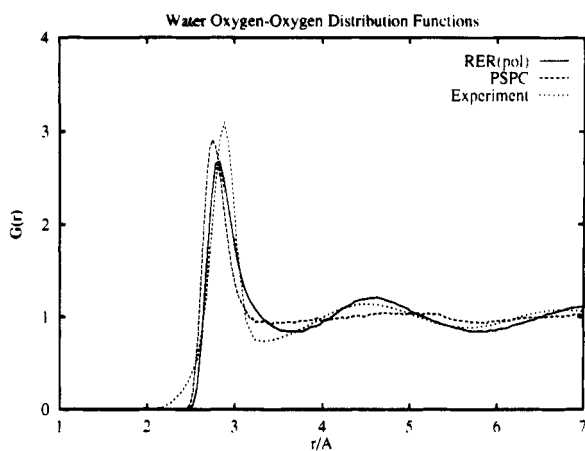


**Figure 5.** Oxygen–oxygen radial distribution function of liquid water for the RER(pol) and PSPC<sup>47</sup> models compared to an experimental data set.<sup>95</sup>

both models. If we instead use the minimum of the model oxygen–oxygen distribution functions, the number of nearest oxygen atoms is 4.6 and 5.2 for the RER(pair) and the RER(pol) models, respectively. Since the running coordination number rises rapidly, a small error in the determination of the location of the minima can perturb these values significantly. The difference of approximately 0.5 appears to be real and is also seen in the temperature studies below. The increase in the number of molecules in the first hydration shell is caused not by an added attraction between molecules, but rather by a softening of the hard core. By modeling the dipole moment using a self-consistent polarization term instead of by using effective charges, we create a more diverse electrostatic environment between pairs of molecules. If we look at the angle,  $\theta$ , between the fixed dipole moment,  $\vec{\mu}_{\text{fix}}$ , arising from the permanent charges and that of the induced dipole moment,  $\vec{\mu}_{\text{ind}}$ , defined as

$$\theta = \arccos\left(\frac{\vec{\mu}_{\text{fix}} \cdot \vec{\mu}_{\text{ind}}}{|\vec{\mu}_{\text{fix}}| |\vec{\mu}_{\text{ind}}|}\right) \quad (12)$$

we find that the half-width of this distribution is  $10^\circ$ . Thus, the induced moments are roughly parallel to the fixed dipole moment. This fluctuation is enough to relax the hydration shell sufficiently to allow for the extra penetration.

In Figures 4 and 5 we compare the nonpolarizable and polarizable models with two other three-site models, the SPC/E and PSPC models. The main difference between these potentials is the positioning of the atomic sites. Our geometry reflects the monomer equilibrium structure whereas the SPC model uses idealized tetrahedral sites. The SPC/E model in Figure 4 gives a tetrahedral ordering that is qualitatively similar to our RER(pair) model, as is evident from the broad peak centered around

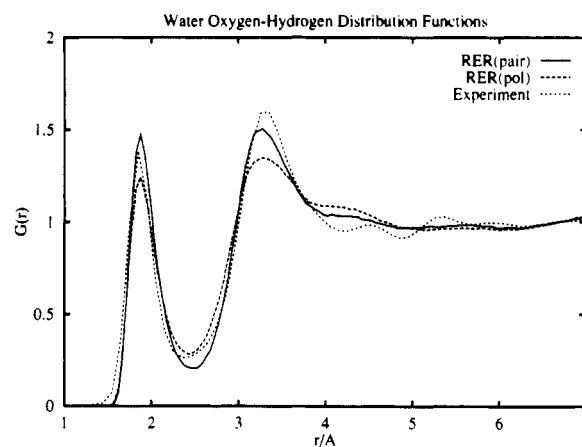


**Figure 6.** Oxygen–hydrogen radial distribution function of liquid water using the developed potentials compared to an experimental data set.<sup>95</sup>

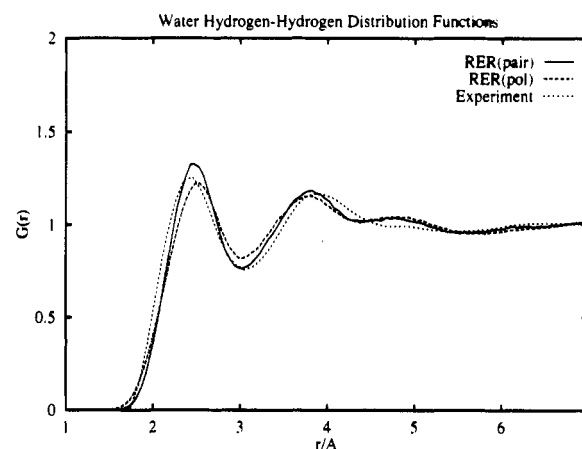


**Figure 7.** Hydrogen–hydrogen radial distribution function of liquid water using the developed potentials compared to an experimental data set.<sup>95</sup>

4.5 Å. The size of a water molecule is shifted toward a smaller radius compared with the nonpolarizable potential and the experimental data. If the repulsion parameter were enlarged in the SPC/E model to account for this defect in size, the peak at 4.5 Å would be diminished and would eventually disappear entirely. An early effort to retain the simplicity of the SPC potential model while incorporating polarization effects is represented by the PSPC model.<sup>47</sup> This model is compared with our polarizable potential in Figure 5. The size of the PSPC water molecule is similar to that of the SPC/E model, but the largest deviation is in the lack of a properly developed tetrahedral structure. The PSPC model cannot be said to give a satisfactory representation of liquid water.

Figures 6 and 7 give the oxygen–hydrogen and hydrogen–hydrogen radial distribution functions for our potentials and the corresponding experimental results. These distributions show good agreement with the experimental data for the peak position of our model potentials. There is some scatter in the predicted intensities. It should be recalled that it is not possible to simultaneously satisfy the experimental oxygen–oxygen and oxygen–hydrogen distances of 2.88 and 1.85 Å, respectively, while using a rigid intramolecular oxygen–hydrogen bond of 0.96 Å.

The new potential models presented here are clearly an improvement over previous three-site models. Given the scatter in the experimental data on water structure, further adjustment of the potentials does not seem warranted.

**3.2. Energies and Pressure.** Liquid water energies evaluated with the proper polarization corrections using eqs 4, 5, and 6 are presented in Table III.

In the polarizable model the average dipole moment of a water molecule in the liquid phase was 2.7 D. Polarization effects from the liquid environment have increased the total dipole moment

TABLE III: Liquid Water Properties at 300 K

potential	$U$ , kJ/mol	$P$ , kbar	$D$ , $10^{-5}$ cm <sup>2</sup> /s	$\tau_1^\mu$ , ps	$\tau_{\text{NMR}}$ , ps
RER(pair) <sup>a</sup>	-41.6	-0.1	2.4	5.8	3.6
RER(pol) <sup>a</sup>	-41.2	-0.2	2.8	4.6	3.4
SPC/E <sup>b</sup>	-41.5	0.0	2.4	5.3	1.9
PSPC <sup>c</sup>	-38.0		2.0	6.3	
experiment	-41.5 <sup>d</sup>	0.0	2.4 <sup>e</sup>	7.5 <sup>f</sup>	2.1 <sup>g</sup>

<sup>a</sup> This work. <sup>b</sup> Berendsen, H. J. C.; Grigera, J. R.; Straatsma, T. P. *J. Phys. Chem.* **1987**, *91*, 6296. <sup>c</sup> Ahlstrom, P.; Wallqvist, A.; Engstrom, S.; Jonsson, B. *Mol. Phys.* **1989**, *68*, 563. <sup>d</sup> Jorgensen, W. L.; Chandrasekhar, J.; Madura, J.; Impey, R. W.; Klein, M. L. *J. Chem. Phys.* **1983**, *79*, 926. <sup>e</sup> Krynicki, K.; Green, C. D.; Sawyer, D. W. *Discuss. Faraday Soc.* **1978**, *66*, 199. <sup>f</sup>  $\tau_{\text{ave}}$ , see text for this estimate. <sup>g</sup> Jonas, J.; DeFries, T.; Wilber, D. J. *J. Chem. Phys.* **1976**, *65*, 582.

0.85 D compared to the monomer value of 1.85 D originating from the partial charges. This is 0.1 D larger than the corresponding fixed, effective dipole moment assigned to the nonpolarizable model.

The pressure of the simulated systems can be calculated from either the atomic or molecular virial without any loss of generality.<sup>85,98</sup> For small water systems of a few hundred particles the natural distribution of instantaneous pressure values is broad. The typical width of normally distributed, independent data points is around 800 bar. Switching the constant-volume conditions to a constant-pressure simulation<sup>99</sup> with a fixed atmospheric pressure, we can instead look at the natural width of the density fluctuations which is then about 0.04 g/cm<sup>3</sup>. This fluctuation, natural to small systems, corresponds to the equivalent volume of eight water molecules in our simulation box. The error in the determined pressure values is of course smaller and depends on how many independent sampling points were generated during the simulation. For the simulations presented here this error corresponds to  $\pm 100$  bar or, equivalently, a volume of one water molecule. The values for the pressure of the RER(pair) and the RER(pol) model systems are given in Table III. Although the values are slightly negative, indicative of an underestimation of the density, no qualitative difference is expected in computer simulations of solution properties. Long-range corrections to the pressure, through tail corrections,<sup>100</sup> are desirable but do not lend themselves to an easy implementation in aqueous systems.

**3.3. Dynamical Properties.** The motion of water molecules in the fluid is characterized by single-molecule dynamical properties such as self-diffusion and orientational time constants.<sup>1,101</sup> Some of these properties are also accessible in computer experiments.<sup>102</sup> The diffusion coefficient was evaluated from the long-time slope of the mean-square displacements of the molecule. These are reported in Table III together with the predictions of some other model potentials and an experimentally determined value<sup>103</sup> at 300 K. The translational motion of the molecules predicted by our new potentials is in the experimental range, with the polarizable potential exhibiting a slightly more diffusive behavior. The difference in translational diffusion between the models is closely coupled to the motion of the entire molecule; i.e., we need to consider an orientational relaxation process.

The rotational motion of water in the liquid is associated with dissipative processes such as dielectric relaxation<sup>104</sup> and intramolecular nuclear magnetic resonance (NMR) relaxation.<sup>105</sup> The corresponding relaxation times can, in principle, be extracted from orientational autocorrelation functions of the appropriate intramolecular vector. The dielectric relaxation experiment measures the reorientation of the macroscopic dipole moment and can tentatively be related to the single-molecule dipole relaxation. This rotational motion is then characterized by the relaxation of the total molecular dipole moment vector  $\hat{\mu}$ . An advantage of the NMR spin-relaxation experiments is that they measure single-molecule properties. The appropriate axis to study in connection with proton NMR measurements is the vector connecting the two hydrogen atoms  $\hat{h}_{\text{HH}}$ . Quadrupole relaxation

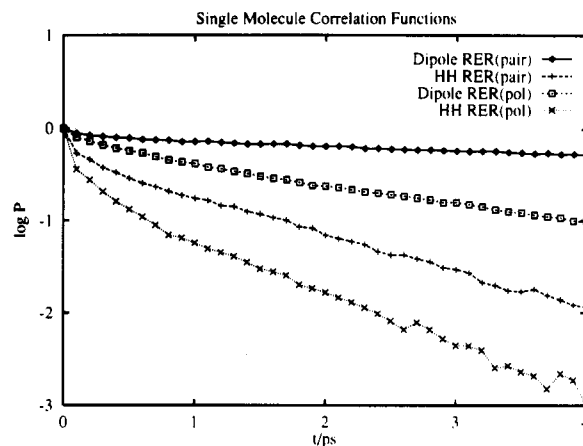


Figure 8. Single molecule correlation functions of the dipole and HH-vector orientational time decay. The logarithm of the corresponding  $P_1^\mu$  and  $P_2^{\text{HH}}$  functions are given for both model potentials.

studies of the <sup>17</sup>O nucleus are associated with the tumbling rate of the oxygen atom and can be characterized by a vector perpendicular to the molecular plane,  $\hat{n}_\perp$ .

The relevant reorientational correlation function for the dipolar relaxation is the first Legendre polynomial

$$P_1^x(t) = \langle \hat{n}_x(0) \cdot \hat{n}_x(t) \rangle \quad (13)$$

whereas for the proton and quadrupole relaxation the second Legendre polynomial

$$P_2^x(t) = \left\langle \frac{3}{2} (\hat{n}_x(0) \cdot \hat{n}_x(t))^2 - \frac{1}{2} \right\rangle \quad (14)$$

were studied, where  $\hat{n}_x(t)$  is the  $x$ th unit vector at time zero and  $\hat{n}_x(t)$  is the same molecular unit vector a time  $t$  later. If we assume a long-time exponential behavior of the relaxation, the corresponding decay times can be calculated from slope of the logarithm of these functions. These functions are shown for the  $\log P_1^\mu(t)$  of the dipole vector and for the  $\log P_2^{\text{HH}}(t)$  of the HH vector in Figure 8 for the RER(pair) and the RER(pol) models, respectively. For the polarizable model the total dipole moment was used.

From Figure 8 we can see that RER(pol) water always relaxes faster than RER(pair) water. The tumbling rate of the polarizable model is larger because the induced moment are faster in responding to local changes in the electrostatic environment. Thus, a polarizable water molecule dynamically changes its dipole moment in response to the environment, whereas a fix charge model cannot. A water molecule with broken hydrogen bonds will have a smaller induced dipole moment and will be more weakly coupled to its neighbors, thereby translating and rotating more freely than in fixed charge models. In this case the free energy barrier to reorientation and hydrogen-bond reorganization will be lower. The overall motion in water is governed by the closely coupled translational and orientational dynamics of water molecules within the first hydration shell. If we compare the diffusion coefficients and relaxation times for the dipole moment  $\tau_1^\mu$  given in Table III, we see that a larger translational motion is associated with a shorter orientational relaxation time. In fact, by forming the root-mean displacements associated with the relaxation time,  $(6D\tau_1^\mu)^{1/2}$ , we find an averaged displacement of 2.9 and 2.8 Å for the RER(pair) and RER(pol), respectively. These values correspond to the average intermolecular distance between two water molecules, as seen in Figure 3.

The measured macroscopic dielectric relaxation time,  $\tau_D$ , is reported to be 8.1 ps.<sup>104</sup> The relationship between the single molecule decay constant  $\tau_1^\mu$ , listed in Table III, and the collective decay time  $\tau_D$  is complex.<sup>106</sup> An estimate of an average microscopic relaxation time can be made under the assumption

of a single experimental macroscopical relaxation time as<sup>107</sup>

$$\tau_{\text{ave}} = \tau_D \kappa^{-1/(2\kappa+1)} \quad (15)$$

where  $\kappa = \epsilon/\epsilon_\infty$ . If the appropriate values for liquid water are used, we can then estimate  $\tau_{\text{ave}}$  to be 7.5 ps, to be compared with the  $\tau_1^\mu$  values listed in Table III for some model potentials. The polarizable potential is somewhat faster than the nonpolarizable model potential, with both showing an enhancement over the estimated relaxation of roughly 30%.

Under the assumption of an exponential relaxation rate,  $P_2^x(t)$  can be written

$$P_2^x(t) = \phi_2^x(t) + A_2^x e^{-t/\tau_2^x} \quad (16)$$

where  $\phi_2^x(t)$  is a rapidly decaying, oscillating function. Thus, the value of the transform at  $t = 0$  is approximated by  $A_2^x \tau_2^x$ .  $A_2^x$  is evaluated from the interpolated intercept at  $t = 0.0$  in Figure 8 using the approximated linear behavior at all times. For the HH vector,  $A_2^{\text{HH}} \tau_2^{\text{HH}}$  should correspond to the relaxation time associated with the intramolecular dipole-dipole coupling.<sup>102</sup> These values, designated  $\tau_{\text{NMR}}$ , are given in Table III for some model potentials together with the experimental values of Jonas et al.<sup>108</sup> Both RER potentials give a similar relaxation behavior. These results overestimate the experimental decay times. A similar analysis of the decay behavior of the out-of-plane vector yields a relaxation time of 1.3 ps for both model potentials, to be compared with the experimental value of 2.4 ps.<sup>109</sup> Consistent with the translational diffusion, the RER(pol) model is as fast or faster in reorienting than the RER(pair) model. The agreement of the reorientational motion with the available experimental data is only fair. It is possible that a better characterization of the quadrupole moment could improve the details of the local dynamics.

**3.4. Temperature Dependence of Model Potentials.** The properties of liquid water are sensitive to temperature changes. Similarly, the model systems presented here will probe slightly different parts of the potential surface and present us with the opportunity to assess the reliability of our potentials. In this study we are focusing on the properties of the fluid in the temperature range between 250 and 350 K, where low temperatures correspond to a supercooled state. Thus, a set of molecular dynamics calculations were carried out in 10 K intervals between 250 and 350 K using the same system of 216 molecules as described above.

**3.4.1. Structure.** Experimental studies of the structure of liquid water have been performed in the supercooled state<sup>92</sup> and for elevated temperatures.<sup>87,89,93,110</sup> In accord with earlier studies of model water systems,<sup>101,111-113</sup> no freezing was observed in any of the studied low-temperature systems.

The structural changes associated with temperature variations can be conveniently reduced by calculating the difference in a pair distribution function relative to a reference state and dividing by the temperature change. This was done for all temperatures relative to the  $T_0 = 300$  K distribution, and an average was thus formed as

$$\frac{\Delta g(r)}{\Delta T} = \left\langle \frac{g_T(r) - g_{T_0}(r)}{T - T_0} \right\rangle \quad (17)$$

where the  $\langle \rangle$  implies an average over all the different temperature simulations. This averaging procedure is done because there is no significant difference between each individual contribution within this temperature range.

The  $\Delta g(r)/\Delta T$  quantity for the oxygen-oxygen pair distribution is plotted in Figure 9 for our model potentials using the room temperature results as a reference state. This data reduction indicates that there are no anomalous structural changes introduced by temperature variations in the 250–350 K range. Within experimental uncertainty, the temperature dependence of the structure is the same for both of our model potentials. The

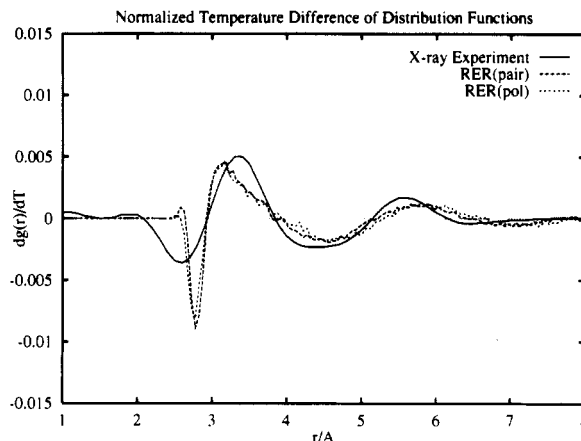


**Figure 9.** Structural variations of the oxygen-oxygen pair distribution functions expressed as  $\Delta g(r)/\Delta T$  with the room temperature results as a reference state. The X-ray data were taken from the work of Bosio et al.<sup>89</sup>

experimentally determined quantity in Figure 9 corresponds to the Fourier transform of the isochoric temperature differential of the X-ray structure factor of heavy water<sup>89</sup>

$$\frac{\Delta g(r)}{\Delta T} = \frac{2}{\pi(T - T_0)} \int_0^\infty Q \langle \Delta S_M(Q, T) \rangle \sin Qr dQ \quad (18)$$

where  $\langle \Delta S_M(Q, T) \rangle$  is the average change in structure factor relative to a reference temperature,  $T_0$ . Thus, the change in the oxygen-oxygen pair distribution function occurring at 3.2 Å is 0.0045 unit/K; i.e., raising the temperature 50 K raises the correlation function 0.225 unit, while decreasing the temperature the same amount decreases the correlation 0.225 unit, relative to the distributions given in Figure 3. The changes occurring at 3.2 Å are associated with the amount of random material present within the idealized tetrahedral structure of a five-membered water cluster. The change at 4.5 Å, the location and hallmark of the tetrahedral ordering in liquid water, is -0.0019 unit/K. That the height at 4.5 Å is 1.171 for the nonpolarizable potential indicates that it is necessary to raise the temperature 90 K above room temperature in order to remove all vestiges of the tetrahedral ordering under the present simulation conditions. The similarity of the structural changes indicates that polarization *per se* does not introduce any abnormalities in the temperature behavior of liquid water. There is a qualitative agreement with the experimental data, except for the region between 2 and 3 Å, which is also the most sensitive to approximations of the form factors used in the experimental data reduction.<sup>97</sup>

A similar data reduction as in eq 17, taking into account neutron scattering lengths of the individual atoms, was also carried out for the weighted average of all distribution functions,<sup>93</sup> i.e.

$$G(r) = 0.091g_{\text{OO}}(r) + 0.421g_{\text{OH}}(r) + 0.489g_{\text{HH}}(r) \quad (19)$$

This averaging emphasizes the oxygen-hydrogen and hydrogen-hydrogen components over the oxygen-oxygen contribution. In Figure 10 these data are given together with a neutron diffraction result reported by Gibson and Dore.<sup>93</sup> Again we can note that the temperature changes are the same for both model potentials. The agreement with experiment is qualitative; i.e., the major structural changes occurring at 1.8, 3.0, 4.5, and 6.0 Å are represented, but their magnitudes are not large enough. At 1.8 Å the only contributing component to the change is the first peak of the oxygen-hydrogen distribution function, as is evident from Figures 6 and 7. In the region between 2 and 3 Å, there is a competition between the density buildup in the first oxygen-hydrogen minimum and the density reduction of the first hydrogen-hydrogen maximum. In the experiments<sup>93</sup> these changes appear to cancel each other out whereas we find a small overall reduction with increased temperature. The large density enhancement at 3.0 Å is due to the increase of the first hydrogen-

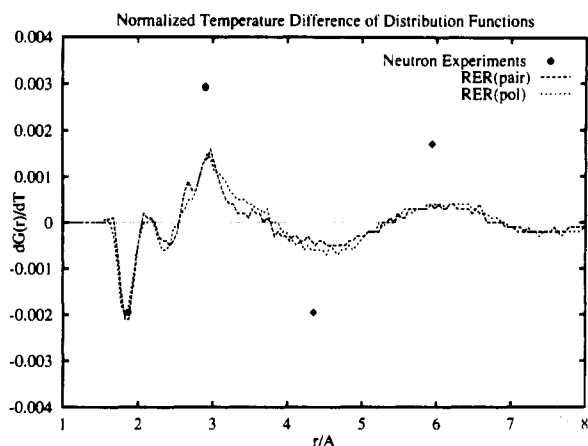


**Figure 10.** Structural variations of the weighted sum of all atom-atom pair distribution function expressed as  $\Delta G(r)/\Delta T$  with the room temperature results as a reference state. The neutron data were read from Figure 4 of the work by Gibson and Dore.<sup>93</sup>

hydrogen minimum. At this distance the contribution from the oxygen-hydrogen distribution vanishes. In the vicinity of the second peak in the oxygen-hydrogen distribution, centered at 3.2 Å, we again have a cancellation between the oxygen-hydrogen and the hydrogen-hydrogen components. The next-nearest molecule correlations between oxygen-hydrogen and hydrogen-hydrogen atoms are located around 4.5 Å and show a decrease of structural components with an increase of temperature. Further out at 6 Å and beyond, the molecular interpretation becomes too complex to unambiguously assign the changes to specific molecular pairs. At these distances the oxygen-hydrogen and hydrogen-hydrogen correlations mainly refer to distant molecules within the hydration shell of a central molecule. The apparent buildup of density in these regions, for the temperature interval considered, reflects the melting of the initially tetrahedrally coordinated hydration shell.

The positions of the first peak in the oxygen-oxygen and oxygen-hydrogen distribution functions do not vary for the nonpolarizable potential within the temperature range studied. The hydrogen-hydrogen peak exhibits a small, 0.05 Å, outward shift in this temperature range for both potentials. What is more important is that the oxygen-oxygen peak does shift approximately 0.03 Å/100 K in the polarizable model liquid, whereas it remains fixed for the nonpolarizable potential. Experimentally this change is somewhat larger, 0.05 Å/100 K.<sup>97</sup>

From the temperature variations of the running coordination number (not shown), we find that there are two isosbestic points. These points indicate that an equal number of water molecules are enclosed within a certain radius regardless of temperature. These are located at 3.23 and 4.52 Å and are associated with 4.2 and 12.5 molecules for the nonpolarizable potential. The corresponding figures for the polarizable potential are 3.23 and 4.57 Å, encompassing 4.2 and 13.1 molecules. These regions do not coincide with the usual definition of hydration shells, i.e., regions between minima of a distribution function. Instead, the location of these radii coincides with the maximum change in intensity with temperature,  $\Delta g(r)/\Delta T$ , of the oxygen-oxygen pair distribution functions. The temperature change thus affects a local density redistribution between the hydration regions.

If instead we calculate how many water molecules are located within the first minimum of the oxygen-oxygen pair distribution function, we can follow the buildup of water coordination. In Figure 11 this property is plotted as a function of temperature for both model potentials. Throughout the temperature range, there is a consistent enhancement of the hydration in the RER(pol) model compared to the RER(pair) model. The temperature variations are smooth, except for the transition between 280 and 290 K for the nonpolarizable and between 330 and 340 K for the polarizable model. The perfect tetrahedral order found in ice,

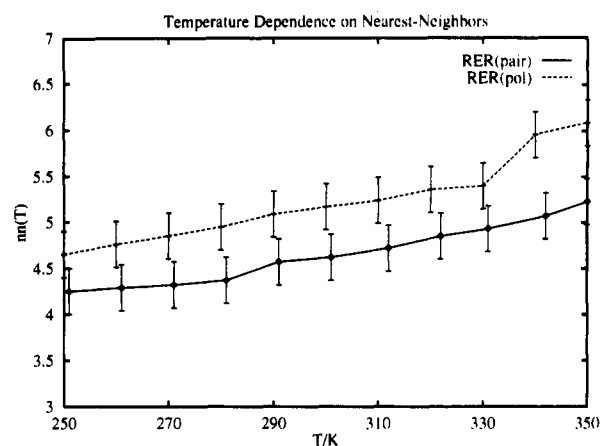


**Figure 11.** Number of nearest water neighbors as a function of temperature for the RER(pair) and RER(pol) models.

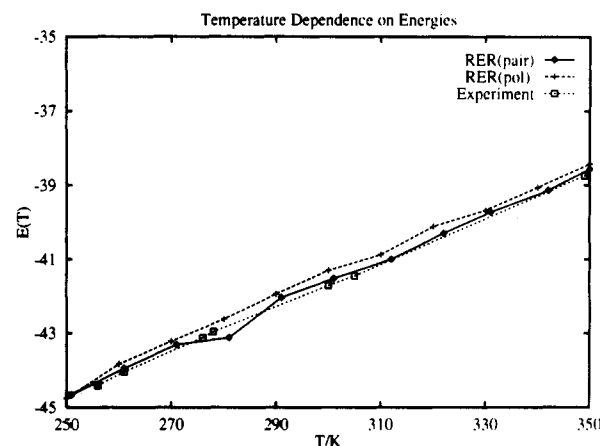


**Figure 12.** Intermolecular potential energy in kJ/mol as a function of temperature.

i.e., with a total number of four nearest neighbors, is never achieved even at the lowest temperature. In this case the self-consistent dipole polarization prevents a successful expulsion of excess water in the first hydration shell. This is due to the effect mentioned above: that fluctuations of the induced dipole moment allow for an easier penetration of the hydration shell, even though the total moment increase and the fluctuations decrease with a lowering of the temperature.

**3.4.2. Energies, Pressure, and Diffusion.** The measured values of the enthalpy of vaporization can be converted into potential energies<sup>6</sup> and are compared with our predictions in Figure 12. This agreement is excellent over the entire temperature range and shows no anomalous behavior. For the polarizable model the induced dipole moment decreases linearly as a function of increase temperature, with a  $d\mu/dT = -1.48 \times 10^{-3}$  D/K. Thus, the maximum total dipole moment is 2.80 D at 250 K and the minimum is 2.65 D at 350 K. These values are all higher than the permanent dipole moment of 2.60 D assigned to the nonpolarizable model. A nominal agreement should occur at 380 K. The reason for the decrease of the dipole moment with increased temperature is that orientational disorder reduces the local electric field and the resulting induced dipoles.

The pressures of the model systems were also monitored and are given in Figure 13. For the polarizable model, the pressure is essentially linear over the entire temperature range, which is consistent with the behavior of a simple liquid. The nonpolarizable potential on the other hand does show an anomalous behavior by exhibiting a broad minimum in the 260–280 K range. The minimum in the pressure curve can be related via the compressibility to a density maximum.<sup>40</sup> Thus, the RER(pair) model does predict a density maximum, though the exact location cannot be precisely determined. The SPC model<sup>63</sup> also exhibits a density maximum. The density maximum in liquid water is associated

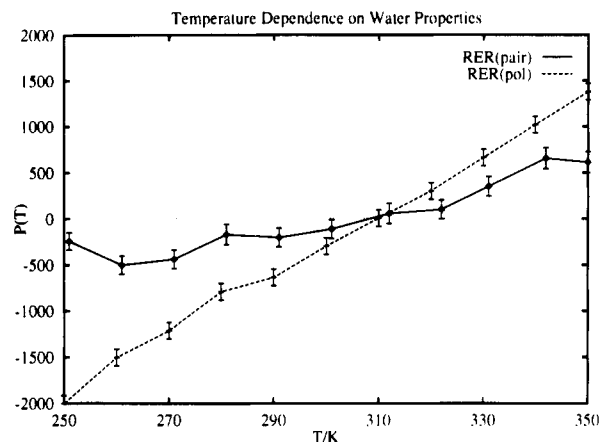


**Figure 13.** Pressure in bar as a function of temperature for the RER(pair) and RER(pol) models.

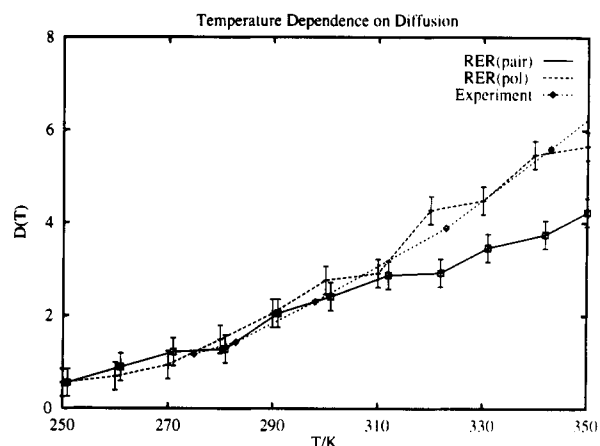


**Figure 14.** Diffusion coefficients in  $10^{-5} \text{ cm}^2/\text{s}$  as a function of temperature for the RER(pair) and RER(pol) models together with experimental data.<sup>103</sup>

with an increased number of nearest neighbors in the first hydration shell, compared to the ideal tetrahedral arrangement of four, combined with a sufficiently low temperature that minimizes the entropy penalty for this arrangement. These requirements are apparently met only for the nonpolarizable potential the 260–280 K temperature range as seen in Figure 11.

The temperature dependence of the translational diffusion coefficient of our model potentials together with the experimental results of Krynicki et al.<sup>103</sup> is shown in Figure 14. The agreement in the temperature region above freezing and up to 310 K is good for both model potentials. The models are in agreement with each other in the supercooled liquid regime. In the region above 310 K the temperature dependence for the two potentials is different, with the RER(pol) potential exhibiting the same qualitative behavior as experiment. The RER(pair) model underestimates the translational diffusion coefficient. At higher temperatures the fluctuations of the dipole moment in the polarizable model becomes even larger than at room temperatures. This further lowers the free energy barriers to translation and rotation compared with the nonpolarizable model and leads to the increased difference between the dynamics of the two models at higher temperatures.

#### 4. Conclusion

By using an effective potential approach, we have constructed two potential models of water by forcing agreement between simulated properties and the known structure, energy, and pressure of the liquid at 300 K. These models are rigid and employ either a pairwise additive functional form or a self-consistent many-body dipole polarizability. In order to maintain a simple, atom-based model, we have been compelled to abandon the traditional

Bernal–Fowler type potentials. Instead, we utilize some ideas of the central force potentials developed by Lemberg, Stillinger, and Rahman<sup>14–16</sup> by letting the potential functional forms vary beyond the traditional  $1/r$ ,  $1/r^6$ , and  $1/r^{12}$  power law expressions.

The advantage of the new models is that they employ only atomic sites and avoid virtual interaction centers. The nonpolarizable model is assigned an effective dipole moment that corresponds to the real dipole moment in the liquid phase and should improve the dielectric response of the model compared to effective models that use an artificially low molecular dipole moment. Indeed, preliminary calculations extending to 1.5 ns using Ewald boundary conditions indicate a dielectric constant of  $83 \pm 6$  for the nonpolarizable model. The model potentials are parametrized to give a satisfactory representation of liquid properties as evident from a clearly resolved tetrahedral hydrogen bond structure and realistic liquid-state energies and pressures. The polarizable model is also parametrized to yield similar liquid properties as the nonpolarizable model. This may allow for the investigation of the effects of using a many-body potential functions on water solution properties. It is also possible to further adjust the presented models by varying the effective potentials,  $V_{\text{eff}}$  and  $V'_{\text{eff}}$ , to create future explicitly density-dependent models.

The predicted dynamical properties at 300 K are in good agreement with the available experimental data. The polarizable potential exhibit a 5–20% faster dynamic behavior compared with the nonpolarizable model. These deviations are only quantitative and cannot be said to constitute a qualitative difference between the two models. Temperature variations in the range between 250 and 350 K reveal structural changes that are compatible with the available diffraction data. Translational diffusion is quantitatively modeled up to 310 K for both models; above this temperature only the polarizable model is able to display the necessary fast motions associated with high-temperature water. This is because fluctuations of the induced dipole moment lowers the free energy barriers that govern the diffusion dynamics.

Our three-site potentials are thus competitive with the state-of-the-art effective liquid-state nonpolarizable potentials such as SPC/E<sup>68</sup> and WK,<sup>61</sup> as well as the polarizable SRWK(pol)<sup>53</sup> model. Quantum chemistry derived potentials, e.g. the NCC<sup>49</sup> and NEMO<sup>51</sup> potential, still give better descriptions of dimer properties, as well as good representations of the liquid.

Vast improvements in the study of liquid water will now be possible only by using a complete quantum mechanical treatment of the system. Until such schemes are generally practicable, classical methods will still be of great interest, both for the pure liquid and in more complex solution systems. As most of the interest in liquid water solutions is focused in a narrow range of temperatures and pressures, effective models parametrized at NTP conditions can be fruitfully employed for these systems. The assumption that effective potentials only see an isotropic surrounding can partly be removed by modeling electric induction effect by a many-body dipole polarizability. Our potentials are ideally suited for these purposes.

**Acknowledgments.** A.W. thanks Profs. A. MacKerell and J. Gao for insightful discussions on liquid water potentials. A careful reading of the manuscript by Dr. M. New is also appreciated.

#### References and Notes

- (1) Eisenberg, D.; Kauzmann, W. *The Structure and Properties of Water*; Oxford University Press: Oxford, 1969.
- (2) Franks, F., Ed. *Water, A Comprehensive Treatise*; Plenum Press: New York, 1972–1982; Vols. 1–7.
- (3) Franks, F., Ed. *Water Science Reviews*; Cambridge University Press: Cambridge, 1986–1988; Vols. 1–3.
- (4) Reimers, J. R.; Watts, R. O.; Klein, M. L. *Chem. Phys.* **1982**, *64*, 95–114.
- (5) Beveridge, D. L.; Mezei, M.; Mehrotra, P. M.; Marchese, F. T.; Ravi-Shanker, G.; Vasu, T.; Swaninathan, S. In *Molecular-Based Study and Prediction of Fluid Properties*; Haile, J. M., Mansoori, G. A., Eds.; Advances in Chemistry Series 204; American Chemical Society: Washington, DC, 1983.

- (6) Jorgensen, W. L.; Chandrasekhar, J.; Madura, J.; Impey, R. W.; Klein, M. L. *J. Chem. Phys.* **1983**, *79*, 926-935.
- (7) Finney, J. L.; Quinn, J. E.; Baum, J. O. In *Water Science Reviews*; Franks, F., Ed.; Cambridge University Press: Cambridge, 1985; Vol. 3, p 93.
- (8) Finney, J. L. *Chem. Scr.* **1989**, *29A*, 123-130.
- (9) Bernal, J. D.; Fowler, R. H. *J. Chem. Phys.* **1933**, *1*, 515-548.
- (10) Sciortino, F.; Geiger, A.; Stanley, H. E. *J. Chem. Phys.* **1992**, *96*, 3857-3865.
- (11) Gorbaty, Y. E.; Demianets, Y. N. *Mol. Phys.* **1985**, *55*, 571-588.
- (12) Gaballa, G. A.; Neilson, G. W. *Mol. Phys.* **1983**, *50*, 97-111.
- (13) Wu, A. Y.; Whalley, E.; Dolling, G. *Mol. Phys.* **1982**, *47*, 603-628.
- (14) Lemberg, H. L.; Stillinger, F. H. *J. Chem. Phys.* **1975**, *62*, 1677-1690.
- (15) Rahman, A.; Stillinger, F. H.; Lemberg, H. L. *J. Chem. Phys.* **1975**, *63*, 5223-5230.
- (16) Stillinger, F. H.; Rahman, A. *J. Chem. Phys.* **1978**, *68*, 666-670.
- (17) Rappé, A.; Goddard, W. J. *Phys. Chem.* **1991**, *95*, 3358-3363.
- (18) Rick, S.; Stuart, S.; Berne, B. J. A flexible charge model of water. Work in progress, 1993.
- (19) Matsubayashi, N.; Wallqvist, A.; Berne, B. J. Flexible vs rigid water models—When is flexibility important in water simulations? Manuscript in preparation, 1993.
- (20) Barrat, J.-L.; McDonald, I. R. *Mol. Phys.* **1990**, *70*, 535-539.
- (21) Smith, D. E.; Haymet, A. D. J. *J. Chem. Phys.* **1992**, *96*, 8450-8459.
- (22) Swanton, D. J.; Backsay, G.; Hush, N. S. *Chem. Phys.* **1983**, *82*, 303-315.
- (23) Swanton, D. J.; Backsay, G.; Hush, N. S. *J. Chem. Phys.* **1986**, *84*, 5715-5727.
- (24) Lie, G. C.; Clementi, E. *Phys. Rev. A* **1986**, *33*, 2679-2693.
- (25) Wallqvist, A. *Chem. Phys.* **1990**, *148*, 439-449.
- (26) Suhm, M. A.; Watts, R. O. *Mol. Phys.* **1991**, *73*, 463-469.
- (27) Wallqvist, A. *Mol. Simulat.* **1991**, *7*, 195-204.
- (28) Kuharski, R. A.; Rossky, P. J. *J. Chem. Phys.* **1985**, *82*, 5164-5177.
- (29) Wallqvist, A.; Berne, B. J. *Chem. Phys. Lett.* **1985**, *117*, 214-219.
- (30) Hankins, D.; Moskowitz, J. W.; Stillinger, F. H. *J. Chem. Phys.* **1970**, *53*, 4544-4554.
- (31) Clementi, E.; Corongiu, G. *Int. J. Quantum Chem.* **1983**, *10*, 31-41.
- (32) Wojcik, I.; Clementi, E. *J. Chem. Phys.* **1986**, *84*, 5970-5971.
- (33) Wojcik, M.; Clementi, E. *J. Chem. Phys.* **1986**, *85*, 3544-3549.
- (34) Hermansson, K. *J. Chem. Phys.* **1988**, *89*, 2149-2159.
- (35) Margenau, H.; Kestner, N. R. *Theory of Intermolecular Forces*; Pergamon: Oxford, 1969.
- (36) Morokuma, K. *J. Chem. Phys.* **1971**, *55*, 1236.
- (37) Ratajczak, H.; Orwilt-Thomas, W. J. *Molecular Interactions*; Wiley: New York, 1980; Vol. 1.
- (38) Axilrod, B. M.; Teller, E. *J. Chem. Phys.* **1943**, *11*, 299-300.
- (39) Rahman, A.; Stillinger, F. H. *J. Chem. Phys.* **1971**, *55*, 3336-3369.
- (40) Stillinger, F. H.; Rahman, A. *J. Chem. Phys.* **1974**, *60*, 1545-1557.
- (41) Gellatly, B. J.; Quinn, J. E.; Barnes, P.; Finney, J. L. *Mol. Phys.* **1983**, *59*, 949-970.
- (42) Krijn, M. P. C. M.; Feil, D. J. *Phys. Chem.* **1987**, *91*, 540-544.
- (43) Stillinger, F. H.; David, C. W. *J. Chem. Phys.* **1978**, *69*, 1473-1484.
- (44) Barnes, P.; Finney, J. L.; Nichols, J. D.; Quinn, J. E. *Nature* **1979**, *282*, 459-464.
- (45) Rullman, J. A. C.; van Duijnen, P. T. *Mol. Phys.* **1988**, *63*, 451-475.
- (46) Sprik, M.; Klein, M. L. *J. Chem. Phys.* **1988**, *89*, 7556-7560.
- (47) Ahlstrom, P.; Wallqvist, A.; Engstrom, S.; Jonsson, B. *Mol. Phys.* **1989**, *68*, 563-581.
- (48) Cieplak, P.; Kollmann, P.; Lybrand, T. *J. Chem. Phys.* **1990**, *92*, 6755-6760.
- (49) Niesar, U.; Corongiu, G.; Clementi, E.; Keller, G. R.; Bhattacharya, D. K. *J. Phys. Chem.* **1990**, *94*, 7949-7956.
- (50) Saint-Martin, H.; Medina-Llanos, C.; Ortega-Blake, I. *J. Chem. Phys.* **1990**, *93*, 6448-6452.
- (51) Wallqvist, A.; Ahlstrom, P.; Karlstrom, G. *J. Phys. Chem.* **1990**, *94*, 1649-1656.
- (52) Wallqvist, A.; Ahlstrom, P.; Karlstrom, G. *J. Phys. Chem.* **1991**, *95*, 4922.
- (53) Sprik, M. *J. Chem. Phys.* **1991**, *95*, 6762-6769.
- (54) Dang, L. X. *J. Chem. Phys.* **1992**, *97*, 2659-2660.
- (55) Kozack, R. E.; Jordan, P. C. *J. Chem. Phys.* **1992**, *96*, 3120-3130.
- (56) Stone, A. J.; Tong, C. S. *Chem. Phys.* **1986**, *137*, 121-135.
- (57) Watts, R. O. *Chem. Phys.* **1977**, *26*, 367-377.
- (58) Reimers, J. R.; Watts, R. O. *Chem. Phys.* **1984**, *91*, 201-223.
- (59) Matsuoka, O.; Clementi, E.; Yoshimine, M. *J. Chem. Phys.* **1976**, *64*, 1351-1361.
- (60) Jorgensen, W. L. *J. Chem. Phys.* **1982**, *77*, 4156-4163.
- (61) Watanabe, K.; Klein, M. L. *Chem. Phys.* **1989**, *131*, 157-167.
- (62) Berendsen, H. J. C.; Postma, J. P. M.; van Gunsteren, W. F.; Hermans, J. In *Intermolecular Forces*; Pullman, B., Ed.; D. Reidel: Dordrecht, 1981; pp 331-342.
- (63) Postma, J. P. M. MD of H<sub>2</sub>O. A molecular dynamics study of water. PhD Thesis, University of Groningen, 1985.
- (64) Wallqvist, A.; Karlstrom, G. *Chem. Scr.* **1989**, *29A*, 131-137.
- (65) Millot, C.; Stone, A. J. *Mol. Phys.* **1992**, *77*, 439-462.
- (66) Sokalski, W. A.; Sawaryn, A. *J. Chem. Phys.* **1987**, *87*, 526-534.
- (67) Andrea, T. A.; Swope, W. C.; Andersen, H. C. *J. Chem. Phys.* **1983**, *79*, 4576-4584.
- (68) Berendsen, H. J. C.; Grigera, J. R.; Straatsma, T. P. *J. Phys. Chem.* **1987**, *91*, 6269-6271.
- (69) Whalley, E. *Chem. Phys. Lett.* **1978**, *53*, 449-451.
- (70) Clough, S. A.; Beers, Y.; Klein, G. P.; Rothman, L. S. *J. Chem. Phys.* **1973**, *59*, 2254-2259.
- (71) Verhoeven, J.; Dymanus, A. *J. Chem. Phys.* **1970**, *52*, 3222.
- (72) Carnie, S. L.; Patey, G. N. *Mol. Phys.* **1982**, *47*, 1129-1151.
- (73) Caillol, J. M.; Levesque, D.; Weiss, J. J.; Kusalik, P. G.; Patey, G. N. *Mol. Phys.* **1985**, *55*, 65-76.
- (74) Patey, G. N.; Levesque, D.; Weiss, J. J. *Mol. Phys.* **1986**, *57*, 337-349.
- (75) Vesely, F. J. *J. Comput. Phys.* **1977**, *24*, 361-371.
- (76) Grey, C. G.; Gubbins, K. E. *Theory of Molecular Fluids*; Clarendon: Oxford, 1984; Vol. 1.
- (77) Thompson, M. J.; Schweizer, K. S.; Chandler, D. *J. Chem. Phys.* **1982**, *76*, 1128-1135.
- (78) van Belle, D.; Lippens, M. F. G.; Wodak, S. J. *Mol. Phys.* **1992**, *77*, 239-255.
- (79) Odutola, J. A.; Dyke, T. R. *J. Chem. Phys.* **1980**, *72*, 5062-5070.
- (80) Curtiss, L. A.; Frurip, D. J.; Blander, M. J. *Chem. Phys.* **1979**, *71*, 2703-2711.
- (81) Szalewicz, K.; Cole, S. J.; Kolos, W.; Bartlett, R. J. *J. Chem. Phys.* **1988**, *89*, 3662-3673.
- (82) Smith, B. J.; Swanton, D. J.; Pople, J. A.; III, H. F. S.; Radom, L. *J. Chem. Phys.* **1990**, *92*, 1240-1247.
- (83) Andersen, H. C. *J. Comput. Phys.* **1983**, *52*, 24-34.
- (84) Swope, W. C.; Andersen, H. C.; Berens, P. H.; Wilson, K. R. *J. Chem. Phys.* **1982**, *76*, 637-649.
- (85) Wallqvist, A.; Teleman, O. *Mol. Phys.* **1991**, *74*, 515-533.
- (86) Chen, S.-H.; Teixeira, J. *Adv. Chem. Phys.* **1986**, *64*, 1-45.
- (87) Narten, A. H.; Levy, H. A. *J. Chem. Phys.* **1971**, *55*, 2263-2269.
- (88) Narten, A. H. *J. Chem. Phys.* **1972**, *56*, 5681-5687.
- (89) Bosio, L.; Chen, S.-H.; Teixeira, J. *Phys. Rev. A* **1983**, *27*, 1468-1475.
- (90) Palinkas, G.; Kalman, E.; Kovacs, P. *Mol. Phys.* **1977**, *34*, 525-537.
- (91) Thiessen, W. E.; Narten, A. H. *J. Chem. Phys.* **1982**, *77*, 2656-2662.
- (92) Bosio, L.; Teixeira, J.; Dore, J. C.; Steytler, D.; Chieux, P. *Mol. Phys.* **1983**, *50*, 733-740.
- (93) Gibson, I. P.; Dore, J. C. *Mol. Phys.* **1983**, *48*, 1019-1030.
- (94) Soper, A. K. *Chem. Phys.* **1984**, *88*, 187-197.
- (95) Soper, A. K.; Phillips, M. G. *Chem. Phys.* **1986**, *107*, 47-60.
- (96) Clementi, E.; Habiz, P. *J. Phys. Chem.* **1983**, *87*, 2815-2820.
- (97) Egelstaff, P. A.; Root, J. H. *Chem. Phys.* **1983**, *76*, 405-420.
- (98) Allen, M. P.; Tildesley, D. J. *Computer Simulation of Liquids*; Clarendon: Oxford, 1987.
- (99) Berendsen, H. J. C.; Postma, J. P. M.; van Gunsteren, W. F.; DiNola, A.; Haak, J. R. *J. Chem. Phys.* **1984**, *81*, 3684-3690.
- (100) Valleau, J. P.; Whittington, S. G. In *Statistical Mechanics A. Modern Theoretical Chemistry*; Berne, B. J., Ed.; Plenum Press: New York, 1977; Vol. 5.
- (101) Stillinger, F. H.; Rahman, A. *J. Chem. Phys.* **1972**, *57*, 1281-1292.
- (102) Impey, R. W.; Madden, P. A.; McDonald, I. R. *Mol. Phys.* **1982**, *46*, 513-539.
- (103) Krynicki, K.; Green, C. D.; Sawyer, D. W. *Discuss. Faraday Soc.* **1978**, *66*, 199-208.
- (104) Hasted, J. B. In *Water, A Comprehensive Treatise*; Franks, F., Ed.; Plenum Press: New York, 1973; Vol. 2.
- (105) Zeidler, M. D. In *Water, A Comprehensive Treatise*; Franks, F., Ed.; Plenum Press: New York, 1973; Vol. 2.
- (106) Berne, B. J.; Pecora, R. *Dynamic Light Scattering*; Wiley: New York, 1976.
- (107) Bottcher, C. J. F.; Bordewijk, P. *Theory of Electric Polarization*; Elsevier: Amsterdam, 1978; Vol. 2.
- (108) Jonas, J.; DeFries, T.; Wilber, D. J. *J. Chem. Phys.* **1976**, *65*, 582-588.
- (109) Halle, B.; Wennerstrom, H. *J. Chem. Phys.* **1982**, *75*, 1928-1943.
- (110) Buontempo, U.; Postorino, P.; Ricci, M. A.; Soper, A. K. *Eur. Phys. Lett.* **1992**, *19*, 385.
- (111) Impey, R. W.; Klein, M. L.; McDonald, I. R. *J. Chem. Phys.* **1981**, *74*, 647-652.
- (112) Karim, O. A.; Haymet, A. D. J. *J. Chem. Phys.* **1988**, *89*, 6889-6896.
- (113) Corongiu, G.; Clementi, E. *J. Chem. Phys.* **1992**, *97*, 2030-2038.